Proceedings of the ASME 2025
International Mechanical Engineering Congress and Exposition
IMECE2025
November 16-20, 2025, Memphis, Tennessee

IMECE2025-165609

SUPPRESSION OF VORTEX SHEDDING FROM A HEMISPHERE BY THE ADDITION OF A POROUS COATING

Satyasreet Jena
University of Cincinnati
Cincinnati, OH

Leonid A. Turkevich
NIOSH
Cincinnati, OH

Milind A. Jog
University of Cincinnati
Cincinnati, OH

Urmila Ghia
University of Cincinnati
Cincinnati, OH

ABSTRACT

Vortex shedding from a bluff body may be suppressed (via a mechanism not fully understood) by coating the body with a porous layer of solid particles. The porous layer alters the boundary layer near the surface of the bluff body, allowing for a more extended transition from no slip at the body surface to the free stream flow; this expansion of the flow profile may be sufficient to stabilize fluctuations in the boundary layer. This may be advantageous in engineering applications where there is a need to reduce aerodynamic forces and acoustic vibrations produced by the fluctuating pressure fields of vortex shedding.

The current study aims to understand the role of the porous layer in suppressing vortex shedding for a hemisphere mounted on a substrate. The simulations are conducted at (hemisphere radius) Reynolds number 10,000. The porous layer is simulated by introducing Lagrangian multiphase solid particles with very high density, arranged as hemispherical shells around the solid dome. The porosity of the layer is controlled by varying the particle diameter, while the thickness of the coating is varied by successively adding shell layers. The simulations are conducted under zero gravitational acceleration; thus, the Lagrangian particles do not settle, but their infinite inertia precludes their being set in motion by the fluid.

Adding a 1-layer shell with 70% porosity significantly reduces the vorticity oscillations at the apex of the hemisphere; at two layers, vortex shedding is eliminated. At increased coating porosity, vortex shedding may still be suppressed with additional coating thickness.

Keywords: Vortex shedding, porous coating, turbulent flow.

NOMENCLATURE

Re	Reynolds Number
ρ	Density
v	Velocity Vector
v_p	Particle Velocity Vector
D_h	Hydraulic Diameter
μ	Dynamic Viscosity
∇	Del Operator
.	Dot Operator
p	Pressure
g	Gravitational Acceleration
k	Turbulent Kinetic Energy
μ_t	Dynamic Eddy Viscosity
I	Identity Tensor
C	Courant Number
St	Strouhal Number
i	x component of quantity
j	y component of quantity
k	z component of quantity

1. INTRODUCTION

When a bluff body is introduced in a fluid flow, a boundary layer and a recirculation zone are set up in the vicinity and the wake of the body, respectively. Above a critical Reynolds number, the boundary layer starts to oscillate and destabilize, releasing localized vortices into the wake. This phenomenon is known as vortex shedding, and when it is structured and periodic, a von Karman vortex street is set up. The shedding of vorticity is accompanied by alternating pressure fields on the body and can give rise to aerodynamic forces, vibrations, and acoustic noises. In engineering applications like bridge cables, chimney columns, and protruding aircraft parts, this phenomenon is undesirable, thus giving rise to the need for the suppression of vortex shedding.

Techniques that suppress or modulate vortex shedding may be either active or passive. As an example of an active method, Hernandez & Pacheco [3] conducted a numerical investigation of 2D flow over a cylinder, where suction was introduced at the front stagnation point. The created sink successfully arrested vortex shedding; they also experimentally validated the results. Mousavi & Kamali [2] numerically and experimentally explored the suppression of vortex shedding and sound pressure levels from a cylinder in a flow using water injection. They showed that, by employing an appropriate flow rate and injection angle of water, vortex shedding and sound pressure levels could be significantly reduced.

Passive methods, on the other hand, offer energy-free solutions that may be more desirable [10-15]. These methods typically involve modifying the geometry of the bluff body, which can perturb the near-wall boundary layer flow. This can be achieved by introducing surface roughness, grooves, helical wires, or dimples on the surface of the body. Mishra & De [1] numerically investigated the suppression of vortex shedding from a cylinder by introducing an on-axis slit across the diameter, separating the cylinder into two hemi-cylinders. The slit geometry and angle were altered, and it was shown that introducing slits can be an effective way of suppressing the vortex shedding. Introducing porous layers is another way of modifying the near-wall flow characteristics. The porous layer spatially extends the velocity variation. Sharma et al. [4] performed LES simulations of a porous coating over a cylinder. The Reynolds number was 1.27×10^5, and the coating thickness and permeability were varied. The study showed that the more permeable layers are sensitive to the coating thickness, while the less permeable layers successfully arrest vortex shedding at a lower thickness. Bruneau & Mortazavi [6] numerically studied a two-dimensional flow over bodies with and without porous layers. They reported strong regularization of the flow and a significant reduction in vortex-induced vibrations. Pereira et al. [7] investigated the flow over a cylinder with and without roughness. The effect of high surface roughness heights was explored, and it was shown that the Strouhal number vanishes depending on the roughness height. Various studies [8-9] have also been conducted on the variation of flow profile over smooth and rough surfaces. These studies are crucial in understanding how modification of the surface affects turbulent flow features.

In the current work, a novel approach has been taken in treating porous coating layers over bluff bodies. Previous work [4,6] models the flow in the porous coating, whereas in this work, the Navier-Stokes equations are solved explicitly for the prescribed structure of the coating. The geometry is of a hemisphere mounted on a substrate, and the porous layer over the hemisphere is modeled by introducing layers of very high-density Lagrangian solid particles. The thickness of the layer is varied by adding more particle layers and the porosity is varied by changing the particle diameters. The combinations that arrest vortex shedding are reported.

2. NUMERICAL MODEL

This section describes the computational domain and the boundary conditions.

2.1 Computational model

The fluid domain for the model is a rectangular cross-section duct, with a length of 88mm, a width of 22mm, and a height of 11mm (Figure 1). The hemisphere is introduced on the bottom surface at a distance of 22mm from the inlet, equidistant from the side walls at 11mm, and has a radius of 2.2mm. The simulations were run primarily in three configurations: the empty duct, the duct with the hemisphere, and finally, the hemisphere with particle layers. The empty duct was used to run a steady-state simulation to obtain the fully developed flow profile in the duct, which is later used as the inlet boundary condition for all subsequent simulations.

The hemisphere was then introduced, and an unsteady case with time stepping of 1×10^{-5} s was simulated. While these time-dependent simulations exhibit acceptable convergence, with residuals $< 10^{-4}$, we note that, with this time-step, the Courant number $C \sim 13$ in some of the volumetrically refined cells of the domain. The transient behavior associated with the initial conditions decays after ~ 30 timesteps. The subsequent time-dependent flow exhibited a von Karman vortex street, with vorticity being shed (periodicity $T = 1.7\times10^{-4}$s) from the apex and either side of the hemisphere. This solid dome solution was used as the initialization for the third case with particle layers (initializing at t=1000 timesteps for the solid dome simulation corresponds to a maximum in the transverse vorticity profile). The particles were introduced as shells covering the hemisphere in a semi-structured pattern. Particles were arranged such that the distance between the particles in the z direction was fixed at 0.06mm; the circumferential distance between adjacent particles within a layer was 0.06mm. The particles were azimuthally staggered between and within layers. Keeping these two parameters fixed, porosity was varied by altering the particle diameters from 5 microns to 50 microns.

2.2 Computational mesh

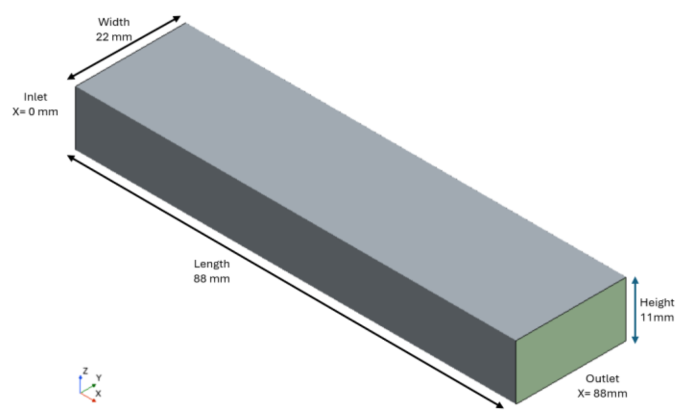

FIGURE 1: COMPUTATIONAL DOMAIN AND ITS DIMENSIONS

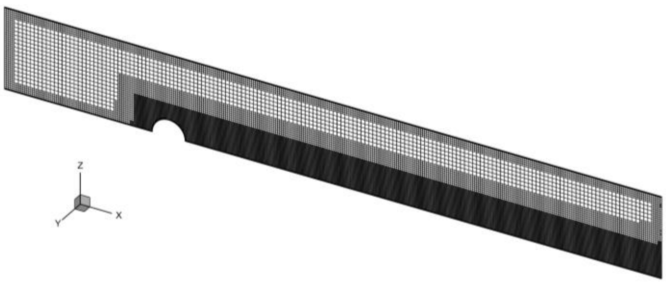

FIGURE 2: MESH AT THE DOMAIN BISECTOR PLANE SHOWING VOLUMETRIC REFINEMENT

A structured trimmed-cell mesh was used to discretize the domain (Figure 2). A volumetric refinement was done near the hemisphere and in its wake to better resolve the fluid flow in that region. Near the walls, prism layer cells, which are orthogonal prismatic cells, were used to better resolve the boundary layer. The target surface size and minimum surface size were set to 50% of the base size, and the surface growth rate was set to 1.001.

A rigorous grid refinement study was conducted on the uncoated hemisphere [5]; 4 grids were considered, with the coarsest having a base size of 1.2mm, and each finer grid had a refinement ratio of 1.5. Two flow regimes were explored, the first being creeping flow and the second at Re~1000. The drag coefficient of the hemisphere was monitored for these 4 grids. The steady state velocity and vorticity were also monitored upstream of the hemisphere. The grid with roughly 2.2 million cells yielded the best apparent order of convergence, with further refinement to 5 million cells causing variation in drag by only 1.8%.

2.3 Boundary conditions and governing equations

The balance of mass through a control volume is expressed by the continuity equation:

$$\frac{\partial \rho}{\partial t} + \nabla.(\rho v) = 0 \tag{1}$$

where ρ is the density and v is the velocity of the fluid. Air is considered to be incompressible, which makes the density constant. Equation 1 can then be reduced to

$$\nabla. v = 0 \tag{2}$$

The resultant force acting on the continuum determines the time rate of change of momentum. The forces can be categorized as body forces, like gravity, and the sum of pressure and shear forces acting on the volume. Accounting for the incompressibility, the momentum equation can be written as follows:

$$\rho\frac{\partial v}{\partial t} + \rho v.\nabla v = -\nabla p + \mu\nabla^2 v + \rho g \tag{3}$$

Here, the first term on the LHS is the local acceleration term and the second term is convective acceleration. On the RHS, the first term is the pressure force, the second term is the viscous force, and the third term is the body force.

The SST (Shear Stress Transport)-k-omega model [16] is used in this study. This model has been shown [17] to accurately reproduce vortex shedding from bluff bodies. By using a blending function, the cross-diffusion term is incorporated in the far field and not near the wall. This approach is thus a blend of the k-epsilon and k-omega models as a function of wall distance.

As mentioned previously, the fully developed flow condition was used as the velocity inlet for the unsteady case. The velocity components, turbulent kinetic energy, and specific dissipation rate were fixed at a velocity inlet condition. The outlet of the domain was set to the 'outlet boundary condition', $\frac{\partial}{\partial x} = 0$; this tends to suppress the flow variation in the x direction, which necessitates extending the domain downstream of the hemisphere.

The fluid forces on the particles can be categorized as surface forces (F_s) or body forces (F_b):

$$m\frac{\partial v_p}{\partial t} = F_s + F_b = F_d + F_p + F_g \tag{4}$$

where v_p is the particle velocity, F_d is the drag force, F_p is the pressure gradient force, and F_g is the gravitational force. The particles were assigned a very high density (1×10^{10} kg/m^3), but gravitational acceleration is set to g = 0. This assignment gives the particles infinite inertia but keeps them from gravitationally settling. Two-way coupling was enabled, which means that the forces exerted by the fluid on the particles in the form of lift and drag were reciprocated equally back to the fluid, and this is added to the Navier-Stokes equation (3) as a volumetric source term for a cell, which is shown in the discrete form:

$$S_v = -\frac{1}{\Delta t}\sum_{\pi}\sum_{\delta t_p} n_{\pi}(F_s + F_b)\delta t_p \tag{5}$$

where the second summation is over all δt_p (particle timestep) for which a particle π is in a cell c, and where n_{π} represents the number of particles in the cell. The summation is over all particles for which two-way coupling is active.

3. RESULTS AND DISCUSSION

This section discusses the results obtained from various simulations.

3.1 Coatings which suppress vortex shedding

The von Karman vortex street that is set up by the uncoated hemisphere is shown in Figure 3. A Q-criterion iso surface is chosen [18], and the surface is colored by vorticity magnitude. Judicious choice of the Q-criterion highlights different structures in the flow. Vorticity is shed periodically from the apex of the hemisphere, and also as a horseshoe vortex encircling the hemisphere. The corners of the duct and side walls also generate vorticity, which shows up as speckles and blots, respectively, in these plots; these domain boundary features are steady-state and are not associated with the dynamic von Karman vortex street from the hemisphere.

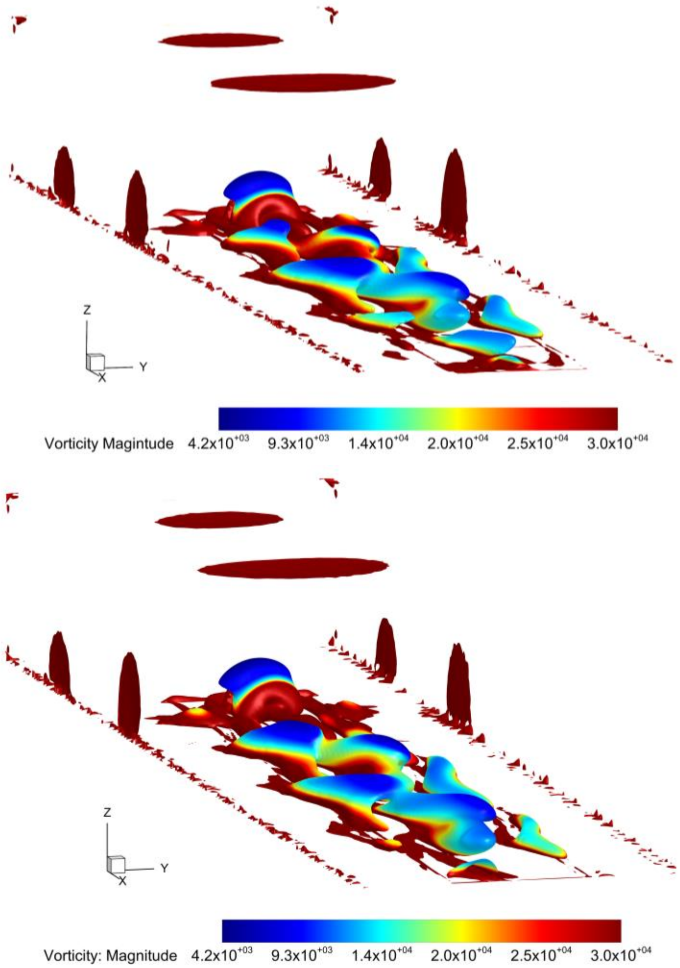

FIGURE 3: Q-CRITERION PLOTS: VON KARMAN VORTEX STREET SHED FROM UNCOATED HEMISPHERE. TOP AND BOTTOM FIGURES ARE SEPARATED BY A TIME INTERVAL OF 8.5×10^{-5}S

The von Karman vortex street set up by the uncoated dome has a periodicity of 1.7×10^{-4}s, corresponding to a Strouhal number St~0.194, close to that of a cylinder, St~0.2. To show the downstream convection of the shed vortex, two snapshots have been shown separated by half a period (Δ t= 8.5×10^{-5}s).

When a coating of appropriate thickness and porosity is applied, the vortex shedding is suppressed, and the flow becomes steady. Figure 4 shows the Q-criterion for a 2-layer 70.77% porosity case where vortex shedding is arrested. The steady-state horse vortex still encircles the hemisphere and decays as it is convected downstream.

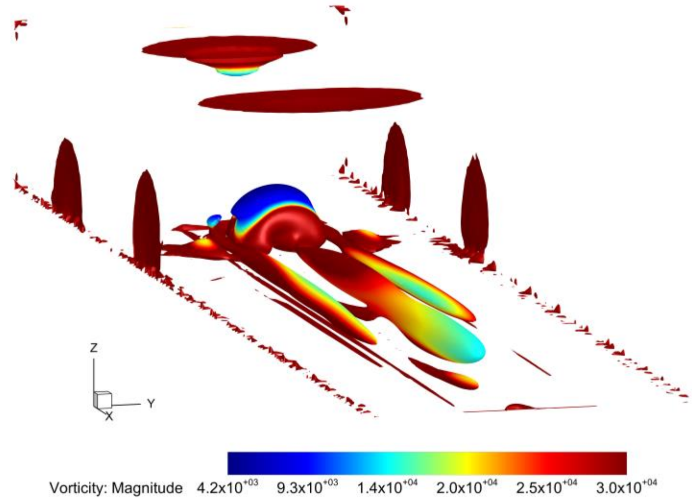

FIGURE 4: Q-CRITERION PLOT: 2-LAYER 50 MICRON (NO SHEDDING)

The y-vorticity near the apex of the hemisphere (approximately 30 ° downstream from the apex on the y = 0 plane) was monitored as a function of time and is shown in Figure 5, comparing various cases. We note that, even after 200 timesteps, there remains a small drift in vorticity of ~ 10 Hz per time step. In fact, for all of the cases studied, the flow exhibits a small but consistent transverse asymmetry, which is seen in non-vanishing x-vorticity and z-vorticity at this monitoring point in the symmetry plane.

There are clear sinusoidal oscillations for the uncoated dome (top panel), with an amplitude (peak to trough) of 9×10^4/s; this represents about ~ 15 % sinusoidal modulations of the steady state vorticity at this location. The comparison to other cases (second panel: 50-micron 1 layer; panels 3-6: 5 microns, 1-4 layers) shows a reduction of the amplitude of these vorticity oscillations at the apex of the hemisphere with the addition of the porous coating. The Strouhal frequency is essentially unchanged.

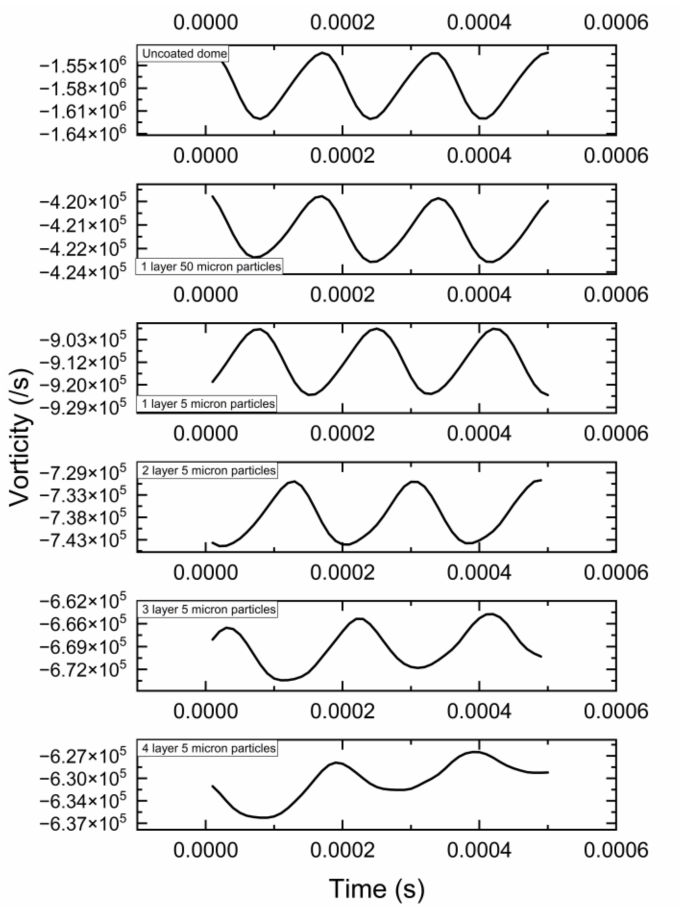

FIGURE 5: VORTICITY VS TIME AT APEX OF HEMISPHERE FOR CASES SHOWING VORTEX SHEDDING

The vorticity amplitude as a function of the number of layers of coating, for 5-micron and 50-micron particles, is shown in Figure 6.

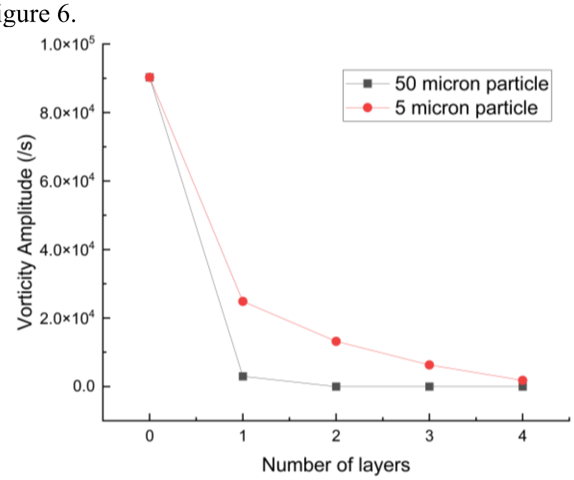

FIGURE 6: VORTICITY AMPLITUDE (PEAK TO TROUGH) VS NUMBER OF LAYERS: 5 MICRON PARTICLES, 50 MICRON PARTICLES

Apex vorticity oscillations, together with Q-criterion plots, were used to identify those cases that support or suppress vortex shedding (Table 1).

Table 1: COMBINATIONS SHOWING VORTEX SHEDDING SUPPRESSION

Particle diameter (microns)	Porosity (%)	Layer 1	Layer 2	Layer 3	Layer 4
50	70.77	O	X	X	X
40	84.98	-	X	-	-
30	93.66	-	X	-	-
20	98.12	-	X	-	-
10	99.76	O	X	X	-
5	99.97	O	O	O	O

The table shows the coating configurations that support or suppress vortex shedding: O indicates that vortex shedding is present; X indicates that vortex shedding is suppressed; - represents that these cases were not considered. For a very porous coating (5-micron particles), more layers are required to suppress vortex shedding than for a less porous coating (50-micron particles).

3.2 Vortex suppression mechanism: altered flow characteristics due to particle coating

We studied the effect of the porous coating on the flow profile near the base of the duct with no hemisphere. The particles are at a distance of 0.06mm from the base, and the particles are spaced by the same distance in the flow direction. In the transverse direction (between lines of particles), the particles are randomly staggered. This construction simulates an amorphous rather than a crystalline coating. Velocity, turbulent kinetic energy, and specific dissipation rate were examined to compare the difference between an uncoated wall and a wall coated by the particle layer.

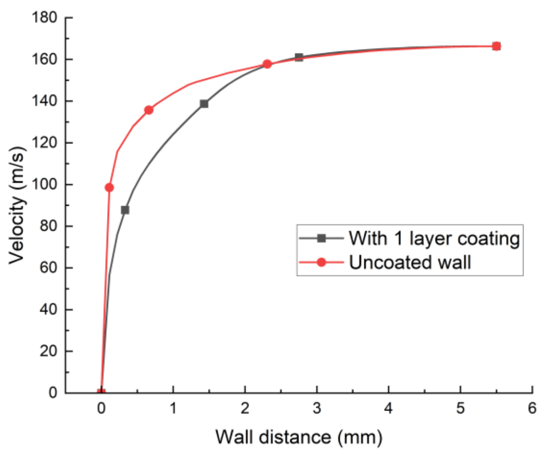

FIGURE 7: VELOCITY PROFILE: UNCOATED WALL, WALL WITH SINGLE LAYER COATING

Figure 7 shows the effect of the coating on the axial velocity profile. Even though the particles are placed at a distance of 0.06mm, the flow is perturbed significantly for distances an order of magnitude larger. Note that this extended length scale is comparable to the size of the bluff body in our study (hemisphere r=2.2mm) that exhibits vortex shedding. We believe that the particles serve as an effective momentum sink and allow for a smoother shear layer compared to the uncoated wall. This has a stabilizing effect and prevents detachment of the boundary layer.

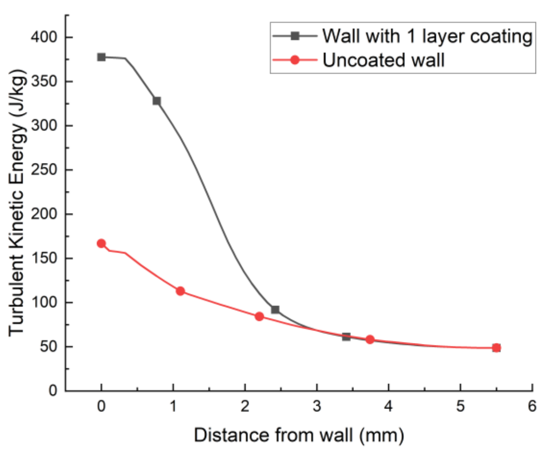

FIGURE 8: TURBULENT KINETIC ENERGY: UNCOATED WALL, WALL WITH SINGLE LAYER COATING

Figure 8 shows that the particles increase the turbulent kinetic energy in the vicinity of the wall. Again, this effect persists on the same length scale as seen in the velocity profile (Figure 7).

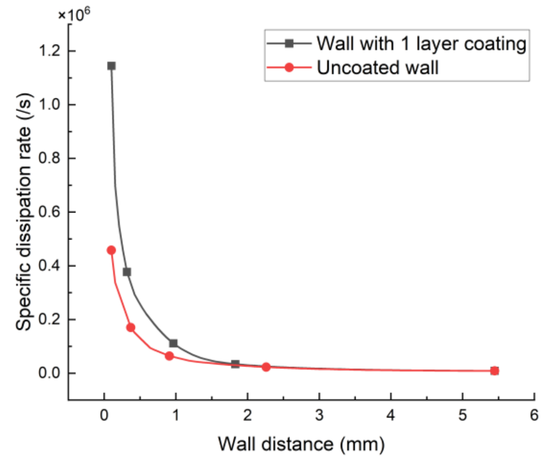

FIGURE 9: SPECIFIC DISSIPATION RATE: UNCOATED WALL, WALL WITH SINGLE LAYER COATING

The specific dissipation rate (Figure 9) also shows a similar, but less pronounced, increase in dissipation due to the porous coating. We believe that the porous coating acts as an effective momentum sink, which dissipates the turbulent kinetic energy, thus suppressing the vortex shedding.

4. CONCLUSION

We have used heavy Lagrangian solid particles to model a porous coating on a bluff body obstructing flow in a rectangular duct. The Strouhal number for the hemisphere was found to be 0.194, which is very close to 0.2 for a cylinder. We have monitored the suppression of vortex shedding as a function of porosity and thickness of the coating, with a less porous coating being able to suppress vortex shedding with fewer layers. We believe that the porous layer acts as a momentum sink and effectively dissipates the turbulent kinetic energy near the surface of the bluff body, thereby suppressing vortex shedding.

5. DISCLAIMER

The findings and conclusions of this paper are those of the authors and do not necessarily represent the views of the National Institute for Occupational Safety and Health, Centers for Disease Control and Prevention. Mention of any product or company name does not constitute endorsement by the National Institute for Occupational Safety and Health, Centers for Disease Control and Prevention.

6. CONFLICT OF INTERESTS

The authors declare that they have no known competing financial interests or personal relationships that could have appeared to influence the work reported in this paper.

REFERENCES

[1] Mishra, A., and De, A., 2021, "Suppression of Vortex Shedding using a Slit through the Circular Cylinder at Low

Reynolds Number," European Journal of Mechanics, B, Fluids, **89**pp. 349–366.

[2] Mousavi, S. M., and Kamali, R., 2020, "Experimental and Numerical Investigation of a New Active Control Method to Suppression of Vortex Shedding and Reduction of Sound Pressure Level of a Circular Cylinder," Aerospace Science and Technology, **103**pp. 105907.

[3] Hernández, R. H., and Pacheco, A., 2002, "Numerical Simulation and Experiments of a Control Method to Suppress the Bénard Von Kármán Instability," The European Physical Journal.B, Condensed Matter Physics, **30**(2) pp. 265–274.

[4] Sharma, S., Geyer, T. F., and Arcondoulis, E. J. G., 2023, "On the Influence of Porous Coating Thickness and Permeability on Passive Flow and Noise Control of Cylinders," Journal of Sound and Vibration, **549**pp. 117563.

[5] Jena, S., 2024, "Computational Analysis of Air Flow Over a Powder Hill," University of Cincinnati

[6] Bruneau, C., and Mortazavi, I., 2008, "Numerical Modelling and Passive Flow Control using Porous Media," Computers & Fluids, **37**(5) pp. 488–498.

[7] Alcântara Pereira, L. A., de Oliveira, M. A., de Moraes, P. G., 2020, "Numerical Experiments of the Flow Around a Bluff Body with and without Roughness Model Near a Moving Wall," Journal of the Brazilian Society of Mechanical Sciences and Engineering, **42**(3) .

[8] Kadivar, M., Tormey, D., and McGranaghan, G., 2021, "A Review on Turbulent Flow Over Rough Surfaces: Fundamentals and Theories," International Journal of Thermofluids, **10**pp. 100077.

[9] Pullin, D. I., Hutchins, N., and Chung, D., 2017, "Turbulent Flow Over a Long Flat Plate with Uniform Roughness," Physical Review Fluids, **2**(8) .

[10] Naito, H., and Fukagata, K., 2012, "Numerical Simulation of Flow Around a Circular Cylinder having Porous Surface," Physics of Fluids (1994), **24**(11) .

[11] Sueki, T., Takaishi, T., Ikeda, M., 2010, "Application of Porous Material to Reduce Aerodynamic Sound from Bluff Bodies," Fluid Dynamics Research, **42**(1) pp. 015004.

[12] Maryami, R., and Naseer, M. R., 2024, "Vortex-Induced Noise Suppression of a Cylinder with Blowing through Porous Media," Physics of Fluids (1994), **36**(6) .

[13] Cheng, Y. T., Sun, J., Chen, P., 2023, "Experimental Study of the Particles Influence on the Pyramid Wake within the Turbulent Boundary Layer," Journal of Applied Fluid Mechanics, **16**(1) pp. 35–46.

[14] Gao, T., Sun, J., Chen, W., 2021, "Experimental Investigation on the Effect of Particles on Large Scale Vortices of an Isolated Hemispherical Roughness Element," Physics of Fluids (1994), **33**(6) .

[15] Li, J., Qiu, X., Shao, Y., 2022, "Turbulent Coherent Structures in Channel Flow with a Wall-Mounted Hemisphere," AIP Advances, **12**(3) pp. 035006–12.

[16] Menter, F. R., 1994, "Two-Equation Eddy-Viscosity Turbulence Models for Engineering Applications," AIAA Journal, **32**(8) pp. 1598–1605.

[17] Zhang, Di., 2017, "Comparison of Various Turbulence Models for Unsteady Flow around a Finite Circular Cylinder at RE=20000" Journal of Physics. Conf. ser. vol 910pp. 012027.

[18] Jeong, J., and Hussain, F., 1995, "On the Identification of a Vortex," Journal of Fluid Mechanics, **285**pp. 69–94.